

Entanglement through qubit motion and the dynamical Casimir effectAndrés Agustí,¹ Enrique Solano,^{2,3,4} and Carlos Sabín¹¹*Instituto de Física Fundamental, CSIC, Serrano, 113-bis, 28006 Madrid, Spain*²*Department of Physical Chemistry, University of the Basque Country UPV/EHU, Apartado 644, 48080 Bilbao, Spain*³*IKERBASQUE, Basque Foundation for Science, Maria Diaz de Haro 3, 48013 Bilbao, Spain*⁴*Department of Physics, Shanghai University, 200444 Shanghai, China*

(Received 4 January 2019; published 20 May 2019)

We explore the interplay between acceleration radiation and the dynamical Casimir effect in the field of superconducting quantum technologies, analyzing the generation of entanglement between two qubits by means of the dynamical Casimir effect in several states of qubit motion. We show that the correlated absorption and emission of photons are crucial for entanglement, which in some cases can be linked to the notion of simultaneity in special relativity.

DOI: [10.1103/PhysRevA.99.052328](https://doi.org/10.1103/PhysRevA.99.052328)**I. INTRODUCTION**

Superconducting quantum technologies together with circuit quantum electrodynamics [1] form one of the most promising candidates for processing of quantum information as well as experimentation on the foundations of quantum mechanics. The advantages of this technology are, on the one hand, the strong coupling between the superconducting qubits and the resonant cavities, as well as the ability to widely tune this coupling and all the parameters of the system, allowing the investigation of new phenomena [2,3] such as, among many others, the dynamical Casimir effect (DCE) [4] or the Unruh effect [5].

The DCE is a member of a large family of effects linked to the quantum fluctuations of the vacuum, among which are the Lamb displacement [6], the magnetic moment of the electron, and the Casimir (static) effect [7–9]. The latter is produced by a reduction in the density of modes imposed by certain boundary conditions, which leads to a pressure of radiation exerted by the vacuum. Its dynamical counterpart shares a similar origin, except for the fact that boundary conditions must be time dependent, which can be achieved by means of SQUIDs [4]. This effect has also been measured by modulating the effective speed of light [10]. On the other hand, the DCE can be considered a resource to generate quantum correlations, including quantum entanglement [11–15]. In this paper, we focus on this feature.

The Unruh effect is another member of the family of aforementioned phenomena, since it consists in the measurement of thermal radiation by a detector moving at constant proper acceleration through the quantum vacuum [16,17]. Unfortunately, this has never been observed since it requires unreachable accelerations to generate detectable signals, although it can be increased by several orders of magnitude when two-level systems are accelerated through resonant cavities by means of nonadiabatic boundary conditions [18]. However, this modification of the original effect is still difficult to reach experimentally and has not been observed. In this report we analyze another scenario: it is possible to simulate the

movement of a qubit in a cavity by modulating the qubit-cavity coupling in the same way the said movement would [19], leading in general to the excitation of qubit and cavity from vacuum as in both variants of the effect. In the same way as with the DCE, this simulation of the Unruh effect can be used as a mechanism for the generation of entanglement [20], only this time between a qubit and the photons of a cavity, not just in the field as in the first effect.

In this paper we consider a scenario where both the DCE and simulated enhanced Unruh radiation can take place (see Fig. 1). It consists of two superconducting resonators sharing a common SQUID and each coupled to a superconducting qubit. DCE radiation can be generated by means of modulation of the magnetic flux threading the SQUID, while the coupling of the qubits can be tuned to simulate their motion. We show that the correlated absorption and re-emission of the DCE radiation by the qubits are crucial for the generation of entanglement, as in the case where the qubits are static [13]. If the motion of the qubit preserves the correlated nature of the absorptions and emissions, entanglement is preserved as well. However, in general, uncorrelated motion of the qubits will result in the vanishing of entanglement, even for low simulated velocities. In the case of equal-length cavities, this physics can be linked to the notion of simultaneity in special relativity: breaking down simultaneity in the absorption would make entanglement vanish.

The rest of the paper is structured as follows. First, in Sec. II we present the superconducting setup, its Hamiltonian, and some relevant features. Then in Sec. III, we discuss the results of, on the one hand, applying perturbation theory to the calculation of the concurrence and, on the other hand, calculating this same magnitude by solving the master equation of the system numerically. Finally, we summarize our conclusions in Sec. IV.

II. SETUP: DCE AND SIMULATED QUBIT MOTION

We consider a system composed of two superconducting qubits—in particular, modifications of the usual design of a

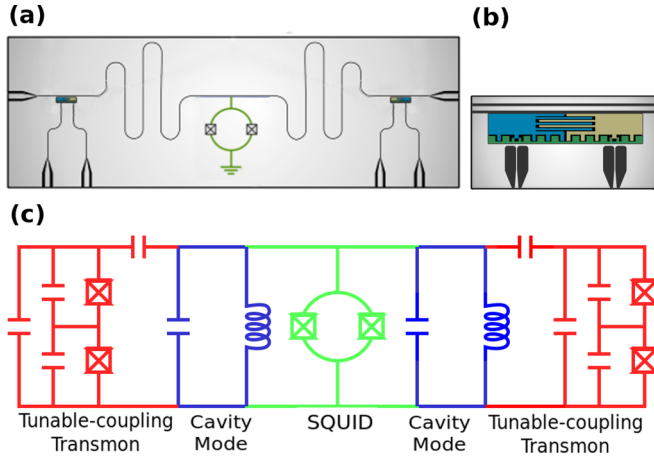


FIG. 1. (a) Scheme of the setup, consisting of two qubits, two resonators, and a SQUID. (b) Scheme of the tunable-coupling transmons. (c) Scheme of the circuit. The qubits (in red) are defined by their characteristic frequencies $\omega_{q_{1,2}}$ and their coupling to the resonators $g_{1,2}(t)$. In blue are indicated the transmission line resonators or cavities, of which only one mode is considered. Their fundamental parameters are their characteristic frequencies $\omega_{c_{1,2}}$ as well as the coupling between them $g_{12}(t)$ due to the SQUID that couples them (in green). The capacitive coupling between cavities and qubits mentioned above is also indicated in red.

transmon qubit [21]—whose coupling to the electromagnetic field can be controlled by the magnetic flux threading the SQUIDs that compose them, which offers the opportunity to simulate the generation of acceleration radiation in the cavity-enhanced Unruh effect. In addition, each of these qubits will interact directly with only one of the modes of only one of the two cavities or transmission line resonators of the system. These resonators interact in turn with each other by means of another SQUID, which allows us to produce time-dependent boundary conditions in the resonators, giving rise to the DCE. An outline of this system is shown in Fig 1.

The Hamiltonian is

$$\begin{aligned}
 H = & \hbar \sum_{i=1}^2 \left[\omega_{c_i} \left(a_i^\dagger a_i + \frac{1}{2} \right) + \frac{\omega_{q_i}}{2} \sigma_i^z \right] \\
 & + \hbar \sum_{i=1}^2 g_i \cos(k_i x_{q_i}(t)) \sigma_i^x (a_i^\dagger + a_i) \\
 & + \hbar g_{1,2}(t) (a_1^\dagger + a_1)(a_2^\dagger + a_2), \quad (1)
 \end{aligned}$$

where the sum runs over both cavities and both qubits. The first line contains the static Hamiltonian, where ω_{c_i} is the frequency of cavity 1 or 2, depending on the subscript, and ω_{q_i} is that of the qubits. On the other hand, a_i^\dagger and a_i are the creation and annihilation operators of the corresponding cavity and σ_i^z is the third Pauli operator of each qubit. The second line of the equation contains the interaction of the qubits with their cavities, where k_i is the wave vector of the cavity, g_i the maximum intensity of its coupling, σ_i^x the first Pauli operator of the qubit, and $x_{q_i}(t)$ the simulated trajectory of qubit motion. Experimentally, the product $k_i x_{q_i}(t)$ is actually $f = \phi(t)/\phi_0$, with ϕ_0 the quantum of magnetic flux and $\phi(t)$ the flux through the SQUID [19,20], which

may be controlled from the outside with a typical nanosecond resolution. The third line contains the interaction between the cavities, $g_{1,2}(t)$ being the time-dependent coupling assuming that the boundary conditions produced by the SQUID do not destroy the structure of normal field modes or make resonances of new modes with the qubits. This is the case when $g_{1,2}(t) = g_0 \cos(\omega_d t)$ with $\omega_d = \omega_{c_1} + \omega_{c_2}$ matching the sum of the cavity mode frequencies. Moreover, in this case the interaction Hamiltonian can be approximated by a two-mode squeezing Hamiltonian [13]:

$$g_{1,2}(t)(a_1^\dagger + a_1)(a_2^\dagger + a_2) \rightarrow g_0/2(a_1^\dagger a_2^\dagger + a_1 a_2). \quad (2)$$

So, finally,

$$\begin{aligned}
 H = & \hbar \sum_{i=1}^2 \left[\omega_{c_i} \left(a_i^\dagger a_i + \frac{1}{2} \right) + \frac{\omega_{q_i}}{2} \sigma_i^z \right] \\
 & + \hbar \sum_{i=1}^2 g_i \cos(k_i x_{q_i}(t)) \sigma_i^x (a_i^\dagger + a_i) \\
 & + \hbar g_0/2 (a_1^\dagger a_2^\dagger e^{i\omega_d t} + a_1 a_2 e^{-i\omega_d t}). \quad (3)
 \end{aligned}$$

Previous work [19] has shown that, even for moderate values of the coupling, the modulation of the coupling strength might resonate with the counterrotating terms of the Hamiltonian. Therefore, we do not perform the rotating wave approximation.

Finally, note that if either or both of the trajectories $x_i(t)$ are changed by $L_i - x_i(t)$ and the relevant coupling constant $g_i \rightarrow -g_i$ is inverted, then the Hamiltonian does not undergo any change, which is quickly deduced using the expression of the cosine of the sum and substituting $k_i = \pi/L_i$. This symmetry can be interpreted as a mechanism by which a path $x_{q_i}(t)$ that passes between the two ends of the cavity in a finite time can be extended beyond that time, reflecting it with respect to the center of the cavity. That is, if for a time τ we have $x_i(\tau) = L_i$ and at a later time $x(\tau + \delta t)$ exceeds L_i , then the path can be modified as $x'_i(\tau + \delta t) = L_i - x_i(\delta t)$, producing the same Hamiltonian which governed the evolution up to τ , except for the sign of g_i . In other words, this symmetry offers a natural bounce condition to continue trajectories that reach the ends of the cavities, so natural that it proves useful throughout the work.

III. RESULTS

We use two methods to analyze entanglement generation in the setup discussed in the previous section, namely, perturbation theory to obtain an approximate expression of the concurrence and then numerical simulations to integrate the master equation governing the system by means of the Python package QuTiP [22]. These two methods make up the following two subsections. In the final subsection, dissipation and temperature are addressed.

A. Perturbative results

The global state $|\Psi(t)\rangle$ under Hamiltonian (3) is expanded up to third order in the couplings g_1 , g_2 , and g_0 from the ground state $|00gg\rangle$, where $|0\rangle$, $|1\rangle$, and so on are the Fock-number states of each cavity and $|g\rangle$ and $|e\rangle$ are the ground

and excited states of each qubit. We aim to compute the entanglement dynamics of the qubits, so it is necessary to trace over the cavity field states, which leads to the density matrix

$$\rho_{\text{qubits}}^{(3)} = \begin{pmatrix} 0 & 0 & 0 & \rho_{14} \\ 0 & 0 & 0 & 0 \\ 0 & 0 & 0 & 0 \\ \rho_{41} & 0 & 0 & 1 \end{pmatrix}, \quad (4)$$

where ρ_{14} is the matrix element $\langle ee|\rho|gg\rangle$ and the nonzero entry on the diagonal corresponds to $\langle gg|\rho|gg\rangle$. For a more detailed derivation refer to the Appendix. Then, using the concurrence $C(\rho)$ [23] as an entanglement measurement, we find

$$\begin{aligned} C(\rho) &= 2|\rho_{14}| = 2|\langle ee|\rho|gg\rangle| = 2|\langle 00ee|\rho_{\text{total}}|00gg\rangle| \\ &= g_1 g_2 g_0 \left| \int_0^t dt_1 \int_0^{t_1} dt_2 \int_0^{t_2} dt_3 \cos(f_1(t_1)) \right. \\ &\quad \times \cos(f_2(t_2)) e^{i\omega_d t_3} \\ &\quad + \int_0^t dt_1 \int_0^{t_1} dt_2 \int_0^{t_2} dt_3 \cos(f_1(t_2)) \\ &\quad \left. \times \cos(f_2(t_1)) e^{i\omega_d t_3} \right|, \quad (5) \end{aligned}$$

where $f_i = k_i x_i(t)$. It should be noted that in this system the concurrence can be interpreted in a very intuitive fashion: it is proportional to the probability that two photons are emitted, one in each cavity, and that each qubit absorbs one. At first sight, Eq. (5) seems to conclude that the qubit motion will only reduce concurrence, since integrating cosines will not provide any further contribution. However, these can cause a resonance, either with each other or with the term due to the emission. In the following paragraphs, we study these resonances produced by different trajectories, paying attention to the conditions that must be fulfilled for their existence.

1. Static qubits

If the qubits are static, Eq. (5) further simplifies, since the cosine functions are all constant. By performing the first integration, we get $\int_0^{t_2} dt_3 e^{i\omega_d t_3} = (e^{i\omega_d t_2} - 1)/i\omega_d$ and the constant term will eventually give rise to

$$C_{\text{rest}} = \frac{g_0 g_1 g_2}{\omega_d} t^2 + O(t). \quad (6)$$

This quadratic behavior of the concurrence seems to be in agreement with [13] for the moderate values of time where the perturbative approach is valid; the perturbative approximation will eventually break down, as we see in detail below.

2. Constant velocity

Particularizing Eq. (5) for the case of qubits moving at constant velocities v_i with initial positions at $x = 0$, we get

$$\begin{aligned} C_{\text{const}} &= \frac{g_1 g_2 g_0}{4\omega_d} \left| \int_0^t dt_1 \int_0^{t_1} dt_2 (e^{ik_1 v_1 t_1} + e^{-ik_1 v_1 t_1}) \right. \\ &\quad \left. \times (e^{ik_2 v_2 t_2} + e^{-ik_2 v_2 t_2}) (e^{i\omega_d t_2} - 1) \right| \end{aligned}$$

$$\begin{aligned} &+ \int_0^t dt_1 \int_0^{t_1} dt_2 (e^{ik_1 v_1 t_2} + e^{-ik_1 v_1 t_2}) \\ &\quad \times (e^{ik_2 v_2 t_1} + e^{-ik_2 v_2 t_1}) (e^{i\omega_d t_2} - 1). \quad (7) \end{aligned}$$

By inspection of Eq. (7), we find that resonances will appear if either or both of the following conditions are verified:

$$\begin{aligned} \omega_d &= k_i |v_i|, \\ k_1 |v_1| &= k_2 |v_2|. \quad (8) \end{aligned}$$

Note that $\omega_d = \omega_1 + \omega_2$, so the above conditions become

$$\begin{aligned} c/L_1 + c/L_2 &= |v_i|/L_i, \\ |v_1|/L_1 &= |v_2|/L_2. \quad (9) \end{aligned}$$

The first one implies a superluminal velocity of at least one of the qubits and was found in [24]. It is related to the emission of Ginzburg radiation at superluminal constant velocities. The second one—since both qubits start in the same position—means that the distance of the qubits to $x = 0$, in units of the corresponding cavity length, is always the same for both qubits, $x_1/L_1 = -x_2/L_2$. Then the Hamiltonians of both qubits are equivalent at any time, entailing that the absorption and re-emission of DCE photons are perfectly correlated. In particular, if the lengths of the cavities are equal $L_1 = L_2$, then the distances are exactly the same, which means that absorptions and emissions always occur simultaneously. This suggests an interesting link between the generation of entanglement in a quantum setup and a key notion of special relativity, such as simultaneity.

When both conditions in Eq. (9) are met at the same time, namely, $|v_1|/L_1 = |v_2|/L_2 = c/L_1 + c/L_2$, then we find

$$C_{\text{const}, 1} = \frac{g_0 g_1 g_2}{\omega_d^2} |\sin(\omega_d t)| t + O(t^0), \quad (10)$$

while if only the first condition is met, $|v_1|/L_1 = c/L_1 + c/L_2 \neq |v_2|/L_2 = kv/\pi$, then

$$C_{\text{const}, 2} = \frac{g_0 g_1 g_2}{2\omega_d kv} |\sin(kvt)| t + O(t^0). \quad (11)$$

In the latter case, it is the velocity of the nonresonant qubit and not the mirror frequency that modulates the generation of concurrence. Even if we assume $kv \approx \omega_d$, then the concurrence in Eq. (11) is reduced by a factor of 1/2 with respect to the concurrence in Eq. (10), which again highlights the importance of the correlations among the absorptions and emissions of photons.

Interestingly, we can use the symmetry of the Hamiltonian described at the end of Sec. I, which in this type of trajectory translates into an inversion of the speed of the qubits when they try to leave the cavities. The full symmetry would change the sign of the relevant coupling, but these signs can be canceled if both trajectories arrive at the ends of the cavities simultaneously and their speeds are then inverted. With these bounces, trajectories of constant velocity can be extended in time. The concurrence, (7), inherits this Hamiltonian symmetry: after n bounces the generated entanglement is n times the entanglement after the first bounce. We see that in this case the simultaneity in the bounce plays a crucial role by simplifying the calculation of the concurrence and extending

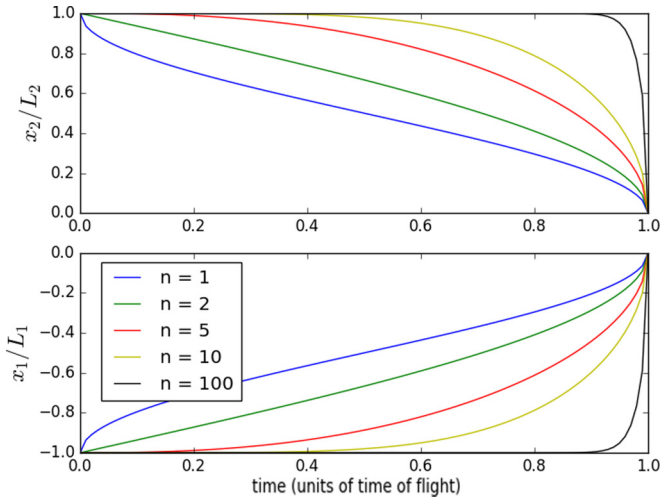


FIG. 2. Trajectories of the qubits, in units of the lengths of their cavities and of the total flight time, for Eq. (12) and $n = 1, 2, 5, 10$, and 100, from higher to lower in the x_1/L_1 subplot.

their relevance. Finally, if the second condition in Eq. (9) is met, but not the first, it is not possible to obtain a closed analytical expression of the concurrence. However, we present numerical results in the next section.

3. Other trajectories

A convenient family of qubit trajectories would be given by

$$\begin{aligned} x_1(t) &= \frac{L_1}{\pi} \arccos \left(2 \left(\frac{t}{\tau} \right)^n - 1 \right), \\ x_2(t) &= -\frac{L_2}{\pi} \arccos \left(2 \left(\frac{t}{\tau} \right)^n - 1 \right), \end{aligned} \quad (12)$$

τ being the flight time of the qubits, namely, the time that it takes for each qubit to traverse its cavity. These trajectories are shown in Fig. 2. They exhibit divergencies in the velocity and the acceleration when the time gets close to the flight time and, also, at $t = 0$ for the particular case $n = 1$.

We find the following concurrence:

$$C_{\arccos} = \frac{4g_0g_1g_2}{\omega_d(n+1)^2 L^{2n}} v^{2n} t^{2n+2} + O(t^{2n}). \quad (13)$$

Therefore, with these trajectories we are able to produce resonances with arbitrary powers of time. Of course, all the above is restricted by the perturbative approximations adopted, which will eventually break down. We now proceed to show results obtained by a numerical integration of the master equation of the system, which enables exploration of the long-time dynamics.

B. Numerical results

1. Static qubits and constant velocities

We consider four trajectories (see Fig. 3). The first is the case where the qubits are static, discussed in [13]. Then we consider the trajectory analyzed perturbatively in the previous section, where the qubits start at $x = 0$ and move at opposite

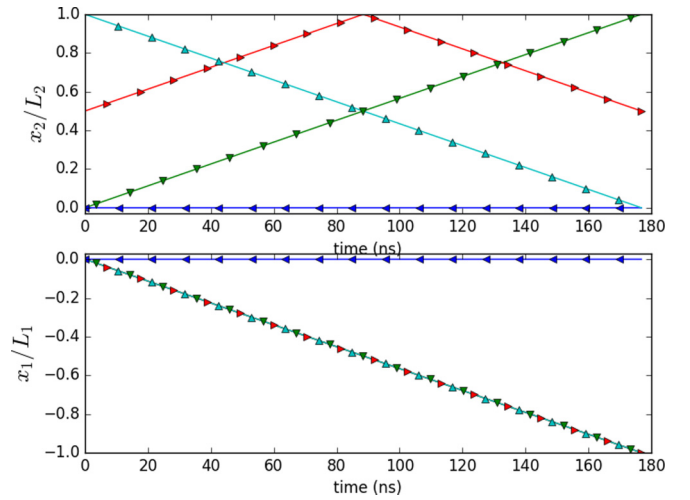


FIG. 3. Qubit trajectories in units of L_i . Dark-blue left-facing triangles: static qubits. Green downward-facing triangles: initial positions $x_i(0) = 0$ and opposite velocities $0.0001(\omega_1 + \omega_2)$. Red right-facing triangles: same velocities as in green but different initial positions, $x_1(0) = 0$ and $x_2(0) = L_2/2$. Cyan upward-facing triangles: same velocities but initial positions $x_1(0) = 0$ and $x_2(0) = L_2$

velocities, giving rise to correlated—simultaneous for equal cavities—absorption and emission of photons. The third case is related to the second by the symmetry relation discussed throughout this work, since one qubit starts at the other end of its cavity. Finally, we consider a trajectory which breaks the correlations among the absorptions and emissions of photons, since one qubit starts out at the center of its cavity while the other starts at 0.

In Fig. 4 we show the numerical results for the concurrences at long times. We reproduce the results for the

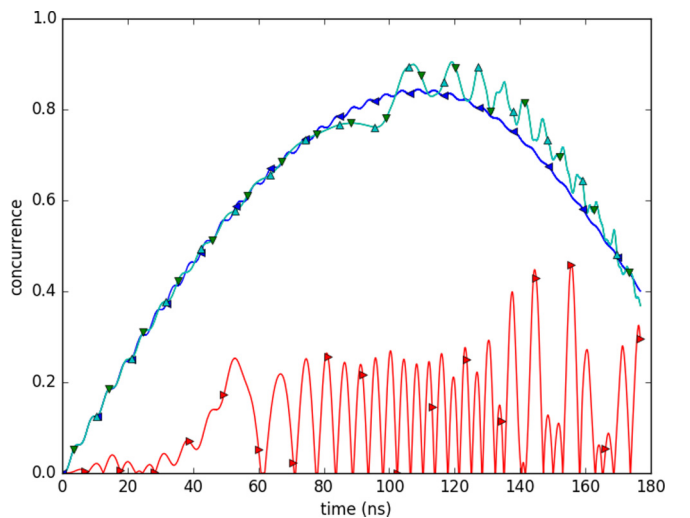


FIG. 4. Concurrences for the trajectories of Fig. 3. The rest of the relevant parameters are $\omega_1/2\pi = 4$ GHz and $\omega_2/2\pi = 5$ GHz for the qubits and cavity modes, with coupling strengths $g_0 = 0.001\omega_1$ and $g_1 = g_2 = 0.04\omega_2$. The maximum values of the concurrence are 0.844, 0.904, 0.461, and 0.904, attained at 108.4, 119.0, 155.6, and 119.0 ns, respectively.

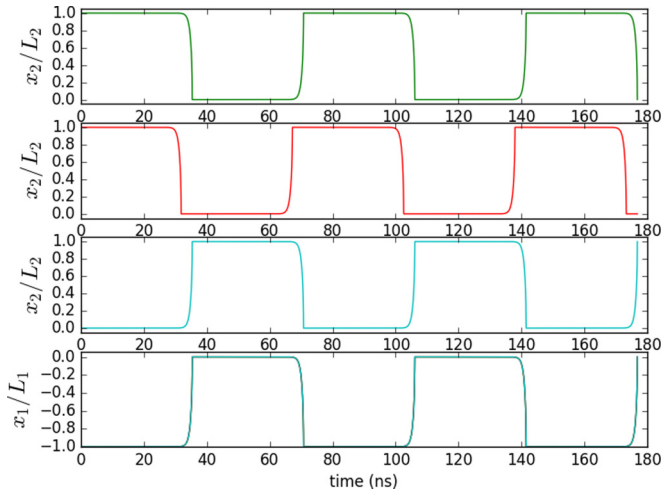


FIG. 5. Qubit trajectories. The bottom plot shows $x_1(t)$ for all cases, as given in (14) for $n = 100$. In the top plot (in green), $x_2(t)$ is given as well by (14). In the second plot (in red), $x_2(t + 0.1\tau)$; and in the third plot (in cyan), $x_2(t + \tau/2)$.

static case in [13] up to the point of maximum concurrence, where they propose to switch off the coupling in order to optimize the entanglement generation. We show that in the two trajectories which preserve the correlated absorptions and emissions the high concurrence is indeed preserved, achieving even larger maximum values. Finally, in the asymmetric case, the concurrence is significantly reduced, as expected. Interestingly, this effect occurs already at low nonrelativistic velocities, which highlights the role of the correlation and simultaneity in the generation of entanglement in this setup. In order to achieve the regime of high velocities, it is convenient to use trajectories similar to the ones in Sec. III A 1. We explore them in the next subsection.

2. Other trajectories

In this case, we have considered the following trajectories (see Fig. 5). We first use trajectories similar to those in Eq. (12), but extended by means of the bounce symmetry:

$$\begin{aligned}
 f_n(x) &= \frac{1}{\pi} \arccos(2x^n - 1), \\
 x_1(t) &= -L_1 f_n\left(\frac{t}{\tau} - \left\lfloor \frac{t}{\tau} \right\rfloor\right) && \text{if } \left\lfloor \frac{t}{\tau} \right\rfloor \text{ even,} \\
 &= -L_1 + L_1 f_n\left(\frac{t}{\tau} - \left\lfloor \frac{t}{\tau} \right\rfloor\right) && \text{if } \left\lfloor \frac{t}{\tau} \right\rfloor \text{ odd,} \\
 x_2(t) &= L_2 f_n\left(\frac{t}{\tau} - \left\lfloor \frac{t}{\tau} \right\rfloor\right) && \text{if } \left\lfloor \frac{t}{\tau} \right\rfloor \text{ even,} \\
 &= L_2 - L_2 f_n\left(\frac{t}{\tau} - \left\lfloor \frac{t}{\tau} \right\rfloor\right) && \text{if } \left\lfloor \frac{t}{\tau} \right\rfloor \text{ odd,} \quad (14)
 \end{aligned}$$

$\tau = v_1/L_1 = v_2/L_2$ again being the time of flight that it takes the qubits to traverse their cavities and $\lfloor x \rfloor$ being the floor function. In this case, as shown in Fig. 5, the trajectories are synchronized in such a way that the absorption and emission of photons is correlated.

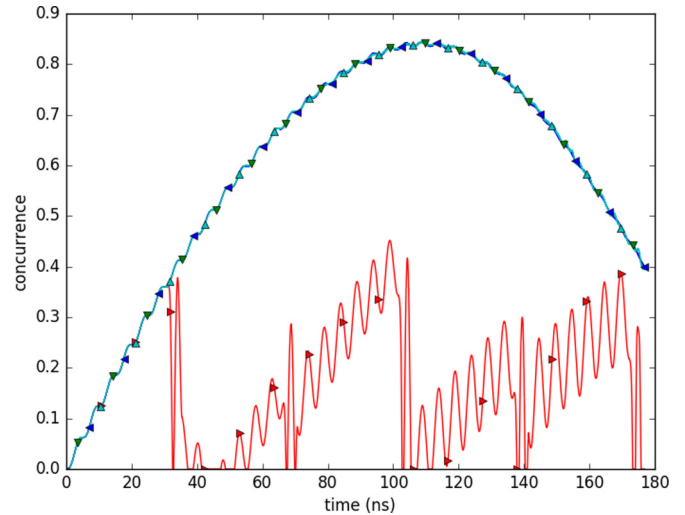


FIG. 6. Concurrences for the trajectories in Fig. 5, using the same color code, but with downward-facing triangles for green, right-facing for red, and upward-facing for cyan. As a reference, we plot the static case in dark blue with left-facing triangles.

Another case that we consider is obtained by replacing $x_2(t)$ with $x_2(t + \tau/2)$ in Eq. (14), which preserves the symmetry between the qubits. Finally, instead making the replacement with, for instance, $x_2(t + 0.1\tau)$, then the qubits are out of phase. We show the concurrences for these trajectories in Fig. 6, which again shows that the correlations and simultaneity between the qubits are crucial to understanding the magnitude of entanglement generation. In order to further illuminate this point, it is interesting to discuss the population in the Bell basis. In the static case and all the cases where the qubit positions are correlated in the way discussed above, photons are emitted and absorbed in pairs, and therefore it is expected that all the population is in the Bell states $|\phi_{\pm}\rangle = 1/\sqrt{2}(|gg\rangle \pm |ee\rangle)$. However, if the positions of the qubits are uncorrelated, it is possible that one of the qubits emits or absorbs a photon, while the other does not. This enables the population of the other Bell states, $|\psi_{\pm}\rangle = 1/\sqrt{2}(|ge\rangle \pm |eg\rangle)$. In Fig. 7 we confirm that this is indeed the case: only in the low-concurrence case does a significant population eventually appear in $|\psi_{\pm}\rangle$. Comparing Figs. 6 and 7, we see that jumps in the population of $|\psi_{\pm}\rangle$ are correlated with falls in the value of the concurrence, as expected.

C. Dissipation and temperature

As a final remark on this analysis, dissipation and temperature must be taken into account. The typical temperature in superconducting circuit experiments is of the order of 10–50 mK, giving a thermal photon number of $10^{-9} - 10^{-2}$. This is clearly neglectable and has not been considered in the calculations. Simulations analogous to those presented in this paper have been run considering relaxation and dephasing times up to 10^4 ns and resonator decoherence times of 10^5 ns, values within experimental reach using superconducting circuit technology [25], as are the values of the rest of the parameters such as characteristic frequencies and couplings.

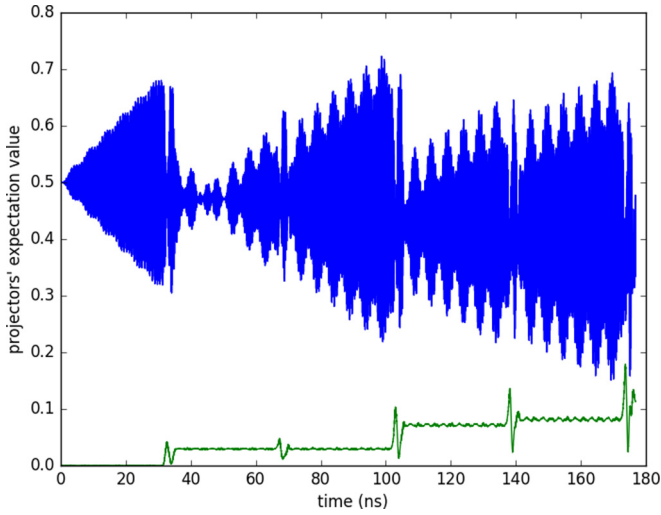


FIG. 7. Expectation value of the Bell-state projectors $|\phi_+\rangle$ (blue; upper plot) and $|\psi_+\rangle$ (green; lower plot). The other Bell states $|\phi_-\rangle$ and $|\psi_-\rangle$ have been omitted given that they take the same values, but with a nanosecond phase difference. Note the remarkable similarity between the dynamics of the concurrence and the Bell-state projector over $|\psi_+\rangle$ in this low-concurrence case.

This dissipation proved to be irrelevant in the dynamics of the system, as initially supposed.

IV. CONCLUSIONS

We have analyzed the entanglement dynamics between two qubits in a system where each one interacts with a resonant cavity with tunable coupling, which allows us to simulate their motion. The cavities interact in turn with each other through a SQUID, which implements a boundary condition that can be modulated by the magnetic flow threading it. This results in a two-mode squeezing Hamiltonian which is the source of entanglement. We show that a high degree of entanglement can be generated both in the case where the qubits are static—discussed in [13]—and in the cases where the motion preserves the fact that photons are absorbed and re-emitted in pairs—one by each qubit—populating only the Bell states $|\phi_{\pm}\rangle$. Otherwise, if the motion of the qubits is such that photons can be emitted or absorbed by only one qubit, we find that the states $|\psi_{\pm}\rangle$ are also populated and the concurrence is dramatically reduced. If the cavities are equal in length, this means that high-concurrence trajectories are characterized by simultaneous absorption and emission of photons, which suggests an interesting link with the notion of simultaneity in special relativity.

These results pave the way for the exploration of special relativistic effects in a quantum setup. For instance, we envision the quantum simulation of the *gedanken* textbook experiments where trains moving at relativistic speeds are used to illustrate the relativity of simultaneity. In our setup, the magnitude of entanglement could be used, in principle, as a witness of simultaneity, and vice versa. Our results are fully within reach with the current technology.

ACKNOWLEDGMENTS

A.A. and C.S. received financial support through the Junior Leader Postdoctoral Fellowship Programme from “la Caixa” Banking Foundation (LCF/BQ/LR18/11640005). E.S. acknowledges support from the projects QMiCS (820505) and OpenSuperQ (820363) of the EU Flagship on Quantum Technologies, Spanish MINECO/FEDER FIS2015-69983-P, and Basque Government IT986-16.

APPENDIX

As pointed out at the beginning of Sec. III A, the global state of both qubits and resonator modes is expanded up to third order in the couplings, which gives nonzero projections onto the states: $\{|00gg\rangle, |11gg\rangle, |10ge\rangle, |01eg\rangle, |00ee\rangle, |22gg\rangle, |21ge\rangle, |12eg\rangle, |33gg\rangle\}$. When performing the partial trace over the fields many of these states (those with the qubits in the same state) will mix, leading to a density matrix with the expression

$$\rho_{\text{qubits}} = \begin{pmatrix} \rho_{11} & 0 & 0 & \rho_{14} \\ 0 & \rho_{22} & 0 & 0 \\ 0 & 0 & \rho_{33} & 0 \\ \rho_{41} & 0 & 0 & \rho_{44} \end{pmatrix}, \quad (\text{A1})$$

where the notation for subscripts is the same as in Eq. (4). The expression of these matrix elements in terms of the perturbative coefficients of $|\Psi\rangle$ are

$$\begin{aligned} \rho_{11} &= \langle ee|\rho|ee\rangle = |c_{00ee}^{(3)}|^2, \\ \rho_{22} &= \langle eg|\rho|eg\rangle = |c_{01eg}^{(2)}|^2 + |c_{12eg}^{(3)}|^2, \\ \rho_{33} &= \langle ge|\rho|ge\rangle = |c_{10ge}^{(2)}|^2 + |c_{21ge}^{(3)}|^2, \\ \rho_{44} &= \langle gg|\rho|gg\rangle = |c_{00gg}^{(0,2)}|^2 + |c_{11gg}^{(1,3)}|^2 + |c_{22gg}^{(3)}|^2, \\ \rho_{14} &= \langle ee|\rho|gg\rangle = c_{00ee}^{(3)*} c_{00gg}^{(0,2)}, \end{aligned}$$

where the superscripts indicate the order in the perturbative expansion at which the coefficient appears—or, in the case of multiple indices, the orders at which new contributions must be taken into account. Notice that since $|\Psi\rangle$ has been expanded up to third order, any term in the matrix elements with a greater power in the couplings (that is, adding their superscripts) must be considered neglectable. With this in mind, the qubits’ density matrix reads

$$\rho_{\text{qubits}} = \begin{pmatrix} 0 & 0 & 0 & c_{00ee}^{(3)*} \\ 0 & 0 & 0 & 0 \\ 0 & 0 & 0 & 0 \\ c_{00ee}^{(3)} & 0 & 0 & 1 \end{pmatrix}, \quad (\text{A2})$$

which proves Eq. (4).

- [1] A. Wallraff, D. I. Schuster, A. Blais, L. Frunzio, R. S. Huang, J. Majer, S. Kumar, S. M. Girving, and R. J. Schoelkopf, *Nature (London)* **431**, 162 (2004).
- [2] O. Astafiev, A. M. Zagoskin, A. A. Abdumalikov, J. Y. A. Pashkin, T. Yamamoto, K. Imomata, Y. Nakamura, and J. Tsai, *Science* **327**, 840 (2010).
- [3] T. Niemczyk *et al.*, *Nat. Phys.* **6**, 772 (2010).
- [4] C. M. Wilson, G. Johansson, A. Pourkabirian, M. Simoen, J. R. Johansson, T. Duty, F. Nori, and P. Delsing, *Nature (London)* **479**, 376 (2011).
- [5] P. D. Nation, J. R. Johansson, M. P. Blencowe, and F. Nori, *Rev. Mod. Phys.* **84**, 1 (2012).
- [6] W. E. Lamb and R. C. Retherford, *Phys. Rev.* **72**, 241 (1947).
- [7] H. B. G. Casimir, *Proc. Akad. Wet. Amsterdam* **51**, 793 (1948).
- [8] S. K. Lamoreaux, *Phys. Rev. Lett.* **78**, 5 (1997).
- [9] U. Mohideen and A. Roy, *Phys. Rev. Lett.* **81**, 4549 (1998).
- [10] P. Lähteenmäki, G. S. Paraoanu, J. Hassel, and P. J. Hakonen, *Proc. Natl. Acad. Sci. USA* **110**, 4234 (2013).
- [11] M. A. Andreatta and V. V. Dodonov, *J. Opt. B* **7**, S11 (2005).
- [12] A. V. Dodonov and V. V. Dodonov, *Phys. Rev. A* **85**, 055805 (2012).
- [13] S. Felicetti, M. Sanz, L. Lamata, G. Romero, G. Johansson, P. Delsing, and E. Solano, *Phys. Rev. Lett.* **113**, 093602 (2014).
- [14] C. Sabín, I. Fuentes, and G. Johansson, *Phys. Rev. A* **92**, 012314 (2015).
- [15] D. N. Samos-Saénz de Buruaga and C. Sabín, *Phys. Rev. A* **95**, 022307 (2017).
- [16] P. Davies, *J. Phys. A* **8**, 609 (1975).
- [17] W. G. Unruh, *Phys. Rev. D* **14**, 870 (1976).
- [18] M. O. Scully, V. V. Kocharovsky, A. Belyanin, E. Fry, and F. Capasso, *Phys. Rev. Lett.* **91**, 243004 (2003).
- [19] S. Felicetti, C. Sabín, I. Fuentes, L. Lamata, G. Romero, and E. Solano, *Phys. Rev. B* **92**, 064501 (2015).
- [20] L. García-Álvarez, S. Felicetti, E. Rico, E. Solano, and C. Sabín, *Sci. Rep.* **7**, 657 (2017).
- [21] S. J. Srinivasan, A. J. Hoffman, J. M. Gambetta, and A. A. Houck, *Phys. Rev. Lett.* **106**, 083601 (2011).
- [22] J. Johansson, P. Nation, and F. Nori, *Comput. Phys. Commun.* **184**, 1234 (2013).
- [23] S. Hill and W. K. Wootters, *Phys. Rev. Lett.* **78**, 5022 (1997).
- [24] C. Sabín, B. Peropadre, L. Lamata, and E. Solano, *Phys. Rev. A* **96**, 032121 (2017).
- [25] M. H. Devoret and R. J. Schoelkopf, *Science* **339**, 1169 (2013).